

A Highly Crystalline Fused-Ring n-Type Small Molecule for Non-Fullerene Acceptor Based Organic Solar Cells and Field-Effect Transistors

Item Type	Article
Authors	Song, Xin;Gasparini, Nicola;Nahid, Masrur Morshed;Chen, Hu;Macphee, Sky Marie;Zhang, Weimin;Norman, Victoria;Zhu, Chenhui;Bryant, Daniel;Ade, Harald;McCulloch, Iain;Baran, Derya
Citation	Song X, Gasparini N, Nahid MM, Chen H, Macphee SM, et al. (2018) A Highly Crystalline Fused-Ring n-Type Small Molecule for Non-Fullerene Acceptor Based Organic Solar Cells and Field-Effect Transistors. Advanced Functional Materials 28: 1802895. Available: http://dx.doi.org/10.1002/adfm.201802895 .
Eprint version	Post-print
DOI	10.1002/adfm.201802895
Publisher	Wiley
Journal	Advanced Functional Materials
Rights	Archived with thanks to Wiley; This file is an open access version redistributed from: https://onlinelibrary.wiley.com/doi/abs/10.1002/adfm.201802895
Download date	2024-02-22 18:45:54
Link to Item	http://hdl.handle.net/10754/630744

DOI: 10.1002/ ((please add manuscript number))

Article type: (Full Paper)

Highly Crystalline Fused-Ring n-Type Small Molecule for Non-Fullerene Acceptor Based Organic Solar Cells and Field-Effect Transistors

Xin Song,¹ Nicola Gasparini,^{*1} Masrur Morshed Nahid,² Hu Chen,¹ Sky Marie Macphee,¹ Weimin
Zhang,¹ Victoria Norman,³ Chenhui Zhu,³ Daniel Bryant,¹ Harald Ade,² Iain McCulloch,^{1,4} Derya
Baran^{*1}

X. Song, Dr. N. Gasparini, S. M. Macphee, Dr. H. Chen, Dr. W. Zhang, Dr. D. Bryant, Prof. I. McCulloch,
Prof. D. Baran

King Abdullah University of Science and Technology (KAUST), KAUST Solar Center (KSC), Division of
Physical Sciences and Engineering, Thuwal, 23955-6900, Saudi Arabia

Corresponding author email: nicola.gasparini@kaust.edu.sa, derya.baran@kaust.edu.sa

Dr. M. M. Nahid, Prof. H. Ade

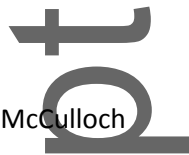
Department of Physics, Organic and Carbon Electronics Lab (ORaCEL), North Carolina State
University, Raleigh, NC 27695, USA

This is the *author manuscript* accepted for publication and has undergone full peer review but has not
been through the copyediting, typesetting, pagination and proofreading process, which may lead to
differences between this version and the [Version of Record](#). Please cite this article as [doi:
10.1002/adfm.201802895](https://doi.org/10.1002/adfm.201802895).

This article is protected by copyright. All rights reserved.

V Norman, Dr. C Zhu

Advanced Light Source, Lawrence Berkeley National Laboratory, Berkeley, CA 94720, USA



Prof. I. McCulloch

Department of Chemistry and Centre for Plastic Electronics

Imperial College London

London SW7 2AZ, UK

E-mail: j.durrant@imperial.ac.uk

Department of Chemistry and Centre for Plastic Electronics

Imperial College London

London SW7 2AZ, UK

E-mail: j.durrant@imperial.ac.uk

Department of Chemistry and Centre for Plastic Electronics, Imperial College London, London SW7 2AZ, UK



Keywords: Fused-ring small molecule, Organic Solar Cells, Organic field-effect transistors, Non-fullerene acceptor, high efficiency



This article is protected by copyright. All rights reserved.

Author Manuscript

Abstract:

N-type organic small molecules (SMs) are attracting attention in the organic electronics field, due to their easy purification procedures with high yield. However, only a few reports show SMs that perform well in both organic field-effect transistors (OFETs) and organic solar cells (OSCs). Here, we report the synthesis and characterization of an n-type small molecule with an indacenodithieno[3,2-b]thiophene (IDTT) core unit and linear alkylated sidechain (C_{16}) (IDTTIC). Compared to the state-of-the-art n-type molecule IDTIC, IDTTIC exhibits smaller optical bandgap and higher absorption coefficient, which is due to the enhanced intramolecular effect. After mixing with the polymer donor PBDB-T, IDTIC based solar cells delivered a power conversion efficiency of only 5.67%. In stark contrast, the OSC performance of IDTTIC improved significantly to 11.2%. We find that the superior photovoltaic properties of PBDB-T:IDTTIC blends are mainly due to: reduced trap-assisted recombination and enhanced molecular packing coherence length and higher domain purity when compared to IDTIC. Moreover, we obtained a significantly higher electron mobility of $0.50\text{ cm}^2\text{V}^{-1}\text{s}^{-1}$ for IDTTIC in OFET devices than for IDTIC ($0.15\text{ cm}^2\text{V}^{-1}\text{s}^{-1}$). These superior performances in OSCs and

This article is protected by copyright. All rights reserved.

OFETs demonstrate that SMs with extended π -conjugation of the backbone possesses a great potential for application in organic electronic devices.

1. Introduction

In the past years, n-type polymers have found widespread use in various organic optoelectronic applications, especially organic field-effect transistors (OFETs) and organic solar cells (OSCs). ^[1-4] However, some common drawbacks of polymers semiconductors, such as: complex purification procedures, the residue of catalysts and batch-to-batch variability, suppress the improvement and repeatability of device performances.^[4-7] N-type small molecules can overcome these drawbacks as the synthesis routes for small molecules eliminate batch to batch variability and the compounds are more easily purified.^[8,9] The most well-known n-type small molecule electron acceptor in OSCs is fullerene and its derivatives, phenyl-C₆₁-butyric acid methyl ester (PC₆₁BM) and its C₇₁ analogue (PC₇₁BM).^[10-12] Yet, weak absorption of fullerenes in the visible region, limited

This article is protected by copyright. All rights reserved.

variability of energy levels and instability under light illumination cannot be easily resolved through structure modifications.^[13] Driven by the need to find alternatives to fullerene, non-fullerene based n-type small molecules such as: naphthodithiophene (NDI), perylene diimide (PDI), dipyrrolopyrrole dione (DPP), are considered as promising materials owing to their tunable molecular structures and energy levels.^[14–20] Among the families of non-fullerene n-type small molecules, the fused-ring electron acceptors (FREAs) have shown rapid progress. This is evident in OSC applications, where the photovoltaic performance of FREAs-based solar cells has reached over 14% in single cells and tandem architecture.^[21–23]

Most of the reported FREAs are based on acceptor (electron-withdrawing)-donor (electron-donating)-acceptor (A-D-A) systems.^[13,24,25] The most prevalent central electron-donating block is a fused-ring conjugated unit composed of: indacenodithiophene (IDT), indacenodithieno[3,2-b]thiophene (IDTT), benzo[1,2-b:4,5-b]dithiophene (BDT) or thiophene-thieno[3,2-b]thiophene-thiophene (4T), where the side chain of these core units mainly consist of alkyl, alkylphenyl or alkylthienyl.^[8,26,27] The most widely used electron-withdrawing blocks are based on either: 3-(dicyanomethylidene)-indan-1-one (IC) or rhodanine units.^[28,29] While a large number of examples of FREAs adopted in OSCs can be found in the literature, the development of high-performance n-type FREAs-based OFETs still lags far behind. One of the reasons is that the alkyl side-chain containing aromatic groups cause steric hindrance and less ordered molecular packing; which has a negative influence of intramolecular hopping, and consequently the performance of OFETs.^[29,30] Previous studies have shown that replacing the side chain containing aromatic groups to linear alkyl chains is a promising way to improve the molecular packing.^[30,31] Following this strategy, Zhan and coworkers reported that IDTIC (also called IDIC), an indacenodithiophene (IDT, five aromatic rings) based small

molecule with liner alkyl chain, facilitates strong crystallinity and high electron mobility.^[6] Another method to enhance the performance of n-type OFETs is to extend the π -conjugated backbone. This can be achieved by introducing more aromatic rings to enhance the intramolecular interaction and therefore extend the planarity of FREAs.^[32,33]

In this study, we combine the strategies of sidechain and backbone modification, reporting the synthesis and characterization of a seven aromatic ring **IDTTIC**, indacenodithieno[3,2-b]thiophene (IDTT) monomer with linear side chain (C_{16}) coupled with 3-(dicyanomethylidene)-indan-1-one (IC) (terminal unit). We demonstrate photovoltaic device efficiencies of 11.2%, without any post-treatment, when IDTTIC is blended with the polymer donor (PBDB-T). Furthermore, we achieve an electron mobility of $0.5\text{ cm}^2\text{V}^{-1}\text{s}^{-1}$ in n-type top gate bottom contact transistors. These results are compared with IDTIC as an exemplary state-of-the-art FREA, highlighting the importance of extending the conjugated backbone.^[34]

2. Results and Discussion

2.1 Materials Synthesis and Properties of NFAs

The structures of IDTIC and IDTTIC are shown in **Figure 1a**. Synthesis routes of C_{16} -IDTTIC are shown in **Scheme 1**. The starting material **1** was prepared according to the literature.^[31] C_{16} -IDTT-dicarbaldehyde **2** was obtained by the Vilsmeier-Haack reaction of **1** in 81% yield. The target acceptor C_{16} -IDTTIC was synthesized by the Knoevenagel condensation reaction of **2** and 3-dihydro-

1H-inden-1-ylidene)malononitrile in 23 % yield. IDTTIC shows good solubility in common organic solvents, such as dichloromethane (DCM), chloroform (CF), chlorobenzene (CB) and dichlorobenzene (DCB). The solution and solid state absorption spectra of IDTIC and IDTTIC are depicted in Figure 1b and 1c, respectively. In solution, IDTIC and IDTTIC exhibit a band onset of \sim 700 nm and \sim 750 nm, respectively. The solid state absorption onset of IDTTIC further bathochromically shifts to \sim 820 nm (70 nm red-shift) corresponding to an optical bandgap of 1.51 eV; whereas the band edge of IDTIC is about 740 nm (40 nm red-shift) with an optical bandgap of 1.68 eV. Furthermore, the extinction coefficient increases for IDTTIC in comparison with IDTIC ($1.50 \times 10^5 \text{ cm}^{-1}$ for IDTIC and $2.49 \times 10^5 \text{ cm}^{-1}$ for IDTTIC, shown in Figure S1), which is due to the stronger intramolecular effect.^[35] By comparison, the normalized absorption spectrum of **PBDB-T** is shown in Figure 1d, demonstrating good spectral complementarity. IDTTIC presents excellent thermal stability (Figure S2) with decomposition temperature (T_d) (5% weight loss) of 349°C via thermogravimetric analysis (TGA), allowing for high temperature thermal annealing in the OFET fabrication process. The obvious two endothermal peaks were observed from 50°C to 250°C in differential scanning calorimetry (DSC) curve (Figure S2b), showing a strong crystallinity of IDTTIC.

The electrochemical properties of IDTIC and IDTTIC are elucidated by cyclic voltammetry (CV). The ionization potential (IP) and electron affinity (EA) of the acceptors energy levels are calculated to be -3.89 eV and -5.85 eV for IDTIC and -3.84 eV and -5.68 eV for IDTTIC by the onset potential of the first oxidative and reductive wave, respectively (Figure 2a, CV curves shown in Figure S3). To verify the origin of the significant upshift in EA level for IDTTIC, we performed calculation using density functional theory (DFT) (Gaussian, wb97xd /6-31G*). For fused-ring small molecules, the electron densities of the highest occupied molecular orbitals (HOMO) are

predominantly localized at the central units, whereas the lowest unoccupied molecular orbital (LUMO) are mainly distributed along the quinoidal conjugation to the terminal acceptor unit.^[27,36] As shown in Figure S4, electron densities of HOMO represent a more delocalized distribution in IDTTIC than that in IDTIC, which is due to the higher concentration of electron-donating thiophene units within the core. This demonstrates that as comparison with that of IDTIC, a higher-lying HOMO level for IDTTIC is formed, which is consistent with the results from CV measurement. It has been shown that the planarity of FREAs has an impact on the charge transport and molecular packing.^[27] The IDTTIC exhibits a flat, planar structure with a dihedral angle between IC and IDTT of $\approx 0^\circ$ (Figure S4). In comparison, IDTIC presents a slightly more twisted structure with the dihedral angle between IC and IDT of $\approx 4^\circ$.

2.2. Device Characterization and Performance Analysis of NFA-OSCs

The effectiveness of IDTIC and IDTTIC as acceptor materials in organic bulk-heterojunction (BHJ) solar cells was then explored. Inverted OSC devices were fabricated with the architecture: indium tin oxide (ITO)/ZnO(~ 40 nm)/PFN-Br(~ 10 nm)/Active layer (~ 150 nm)/MoO_x(~ 7 nm)/Ag (100 nm). We selected PBDB-T (Figure 1a) as a donor polymer because of its complementary absorption and well matched energy levels with IDTIC and IDTTIC.^[24,37] The optimization details, including thickness, donor/acceptor ratio, and interfacial modification, are presented in the Supporting Information. The characteristic current density-voltage (*J*-*V*) curves under illumination AM 1.5 G at 100 mW cm⁻² of the champion devices (PBDB-T:IDTIC and PBDB-T:IDTTIC) are presented in Figure 2b, and corresponding device parameters are summarized in **Table 1**. As shown, the short-circuit current density (*J*_{sc}), open-circuit voltage (*V*_{oc}) and fill factor (FF) of IDTTIC based devices were significantly higher than that of IDTIC based devices - in line with the higher absorption strength and higher lying

LUMO level discussed earlier. External quantum efficiencies (EQE) measurements were conducted by the IDTIC and IDTTIC based devices and the data are shown in Figure 2c. The integrated J_{sc} values are well matched with the data from solar simulation with the error smaller than 5% (Table 1). Due to the wider absorption range (Figure 3d) of PBDB-T: IDTTIC blend, the corresponding devices showed a broader light response than that of IDTIC devices, which is consistent with the EQE curves. In detail, the OSC device based on PBDB-T:IDTTIC exhibits a broad photon response extending to 820 nm with EQE values (over 70%), while PBDB-T:IDTIC-based OSC shows a limited absorption range from (300 nm to 750 nm) and much lower EQE (values lower 65%) in the whole absorption spectrum, proving in part that the higher current density obtained from IDTTIC based devices is due to the broader absorption range (can be seen in Table 1, extrapolated current density).

By analyzing photocurrent density (J_{ph}) as a function of effective voltage (V_{eff}), we can evaluate charge generation and transport loss, which has a strong relationship with the J_{sc} and FF. In detail, J_{ph} is equal to $J_I - J_d$, where J_I and J_d are the current density under illumination at 100 mW cm⁻² and in the dark, respectively. V_{eff} is given by $V_{eff} = V_0 - V$, where V_0 is the compensation voltage defined as $J_{ph}(V_0)=0$, and V is the applied voltage.^[19] As shown in Figure 3a, the current-voltage plots indicate that for PBDB-T:IDTTIC devices, J_{ph} quickly saturates for V_{eff} below 0.5 V, whereas PBDB-T:IDTIC devices depicts a strong dependence of J_{ph} with V_{eff} . In saturation condition, we can estimate the maximum generation rate of free charge carriers G_{max} according to the equation: $J_{sat}=qG_{max}L$, where q is the electronic charge and L is the active layer thickness.^[19] In agreement with the J_{sc} values obtained at 1 sun illumination, we calculate G_{max} values of 7.11×10^{21} and 1.21×10^{22} cm⁻³s⁻¹ for IDTIC and IDTTIC-based devices, respectively, confirming the better photon-to-current conversion for PBDB-T:IDTTIC solar cells. By following the charge generation at the voltage V_{MPP} (MPP: maximum

power point of J - V curve) and under short-circuit conditions ($V=0$), we observe the stark contrast between these acceptors. At $V=0$, the charge generation and collection rate achieve values of 59% and 90% of G_{max} for IDTIC and IDTTIC based devices, respectively. Similarly, at $V=V_{MPP}$, we obtain G_{mpp} values of 38%, and 88% of G for PBDB-T:IDTIC and PBDB-T:IDTTIC solar cells, respectively. The huge difference in G values in the two NFA-based solar cells reflects the FF and J_{sc} limitation of IDTIC compared to IDTTIC blends.

To further investigate the charge recombination mechanism, we carried out light intensity current-voltage measurements to study the evolution of J_{sc} and V_{oc} for a wide range of light levels. J_{sc} generally follows a power law dependence on light intensity according to $J_{sc} \propto P_{in}^S$, where S is a power law exponent and P_{in} is the light intensity. In general, a linear dependence, i.e. $S=1$ is observed for solar cells not limited by bimolecular recombination, whereas $S<1$ suggests bimolecular recombination.^[38] Figure 3b shows the relationship of the J_{sc} vs light intensity for PBDB-T:IDTIC and PBDB-T:IDTTIC devices. We calculate S of 0.95 and 1.00 for IDTIC and IDTTIC-based devices, respectively, suggesting higher bimolecular recombination in PBDB-T:IDTIC; leading to low carrier extraction and consequentially lower J_{sc} compared to PBDB-T:IDTTIC solar cells. Light-induced V_{oc} losses are thought to be attributed to trap assisted recombination. The signature of trap-assisted recombination or monomolecular recombination depicts a slope of $2 kT/q$ (thermal voltage at 300 K) in the plot of V_{oc} versus the natural logarithm of the light intensity. Conversely, bimolecular recombination is reflected in a slope of kT/q .^[39] As observed in Figure 3c, the slopes of V_{oc} vs light intensity plots for PBDB-T:IDTIC and PBDB-T:IDTTIC devices are 1.32 and 1.05 kT/q respectively, indicating that trap states in IDTIC-based devices have a detrimental effect on the transport properties of the devices, in agreement with the lower FF value obtained compared to IDTTIC-based

solar cells. Consequently, we conclude that charge extraction in PBDB-T:IDTIC is limited by trap-assisted recombination, whereas IDTTIC-based devices do not suffer from this limitation.^[40]

We now turn our focus on the transport properties of PBDB-T:IDTIC and PBDB-T:IDTTIC blends. The charge carrier mobility (space-charge limited current method, SCLC) of the blends is calculated by fitting the J -Vs from corresponding electron-only and hole-only devices in the dark condition (Figure S10). According to the SCLC model, we obtained electron mobility of $5.51 \times 10^{-5} \text{ cm}^2\text{V}^{-1}\text{s}^{-1}$ and $1.15 \times 10^{-4} \text{ cm}^2\text{V}^{-1}\text{s}^{-1}$ for PBDB-T:IDTIC and PBDB-T:IDTTIC blends, whereas similar hole mobility ($2.3 \times 10^{-4} \text{ cm}^2\text{V}^{-1}\text{s}^{-1}$) was obtained for the two blends (Table 1). PBDB-T:IDTTIC blend presents improved and more balanced hole/electron mobilities than that of PBDB-T:IDTIC, which is partly due to the more ordered molecular packing (discussed in GIWAXS part).^[41]

To further check recombination kinetics of the two blends, we used transient measurements and in particular photo-induced charge carrier extraction by linearly increasing voltage (Photo-CELIV) measurements.^[42] Notably, this method is widely used for measuring the charge carrier mobility (μ) as well as charge recombination rates, with the advantage of the measurements being carried out on the same devices used for J -V and EQE, making the data directly comparable. Figure S11 shows the Photo-CELIV traces of IDTIC and IDTTIC-based devices as a function of the delay time (t_d), with the carrier mobility of $1.5 \times 10^{-4} \text{ cm}^2\text{V}^{-1}\text{s}^{-1}$ (PBDB-T:IDTIC) and $2.6 \times 10^{-4} \text{ cm}^2\text{V}^{-1}\text{s}^{-1}$ (PBDB-T:IDTTIC), respectively.^[17] Calculating Photo-CELIV as a function of the delay time t_d allows insight into the recombination kinetics of charge carriers and the calculation of the bimolecular recombination coefficient (β) according to equation:

$$n(t) = \frac{n_0}{1 + n_0 \beta t} \quad (1)$$

This article is protected by copyright. All rights reserved.

where $n(t)$ is the charge density at time t and n_0 is the initial charge density. By fitting n vs t_d from equation 1, we calculate β of $2.3 \times 10^{-10} \text{ cm}^3 \text{s}^{-1}$ and $4.5 \times 10^{-11} \text{ cm}^3 \text{s}^{-1}$ for PBDB-T:IDTIC and PBDB-T:IDTTIC devices, respectively. Moreover, according to the Langevin model, the recombination rate of electron and a hole can be described with the Langevin recombination coefficient by $\beta_L = \frac{q * (\mu_h + \mu_e)}{\varepsilon_0 * \varepsilon}$, where μ_h and μ_e are the effective charge carrier mobility of holes and electrons, respectively, ε_0 is the vacuum and ε the relative permittivity.^[43] Due to the intrinsic lower mobility of organic semiconductors compared to the inorganic counterparts the bimolecular recombination rate of holes and electrons, usually referred to as Langevin recombination, and is typically considered an important loss mechanism. Differently, $\beta/\beta_L < 1$ indicates reduced Langevin recombination, i.e. the bimolecular recombination is not instant as they meet and an electron hole pair has a significant chance to split again.^[44] We calculated $\beta_L = 1.88 \times 10^{-10} \text{ cm}^3 \text{s}^{-1}$ and $2.73 \times 10^{-10} \text{ cm}^3 \text{s}^{-1}$ for PBDB-T:IDTIC and PBDB-T:IDTTIC, which is in agreement with values reported for other organic photovoltaics (Figure 3d). The resulting ratio β/β_L for PBDB-T:IDTIC and PBDB-T:IDTTIC blends of 1.22 and 0.16, respectively, confirm the lower recombination losses in IDTTIC based devices as being the origin of the higher FF and overall higher PCE over IDTIC-based blends.^[45]

In bulk heterojunction solar cells, morphology and molecule orientation critically impact the carrier generation and transport, which has a significant influence on the efficiency. Utilizing a combination of grazing-incidence wide-angle X ray scattering (GIWAXS) and resonant soft X-ray scattering (R-SoXS) experiments, to study the influence of backbone substitutes on the molecule packing and morphological properties of the blends, is well understood.^[46–49] Figure 4a and b show 2D GIWAXS patterns of NFA neat films of IDTIC and IDTTIC, respectively, where very highly ordered packing motifs are readily evident.^[50,51] Figure 4c and 4d present the GIWAXS patterns of PBDB-

T:IDTIC and PBDB-T:IDTTIC blend films. Notably, the highly ordered IDTIC and IDTTIC crystallites were largely suppressed when they are blended with PBDB-T. While this suppressed scattering remains obvious, both of the blends showed sufficient scattering profiles, especially in the OOP direction that allowed further analysis (ca. **Table 2**). Figure 4e (and S14c) shows OOP (and IP) 1D GIWAXS profiles of these blends (along with the PBDB-T neat film) where several orders of alkyl stacking peaks are seen. Interestingly however, a stark contrast is observed in the OOP π - π stacking peaks that are assigned to the NFAs in the blend films; see Supporting Information (Figure S12) for details. In particular, PBDB-T:IDTIC film shows π - π stacking coherence length of \sim 1.3 nm; in sharp contrast, PBDB-T:IDTTIC exhibits 3.5-times larger coherence length (4.60 nm). As previously shown by Ade and coworkers, the π - π coherence length may have a positive correlation with the FF in a monotonic trend.^[46] In our case, IDTTIC blend film shows a pronounced longer coherence lengths than that from IDTIC blend, which is in good agreement higher FF obtained in IDTTIC devices.

The morphology and length scale of blend films are also characterized by R-SoXS measurements.^[52] Figure 4f shows the Lorentz-corrected R-SoXS profiles of both the blends; the profiles of PBDB-T:IDTIC blend features the predominant peaks location at $q \sim$ 0.07 nm⁻¹ which corresponds to a length scale (center-to-center spacing) of ca. 80 nm. The length scale of PBDB-T:IDTTIC blend is found to be similar (\sim 84 nm). Interestingly however, the mean-square composition variations, which relates to domain purity and serves as a fundamental metric of exciton generation and charge transport of the corresponding blend films, is found to be more than 2-times higher in IDTTIC blend film when compared to IDTIC based film.^{[53][54]} The morphological features of blend films were also characterized via atomic force microscopy (AFM). As shown in Figure S15, considering the high crystallinity of IDTIC and IDTTIC, both of PBDB-T:IDTIC and PBDB-T:IDTTIC show

clear phase separation with small root-mean-square (RMS) roughness of 3.68 nm and 2.92 nm, respectively. This finding of larger coherence length (from GIWAXS) and higher (relative) domain purity (from R-SoXS) directly corroborates to the improved J_{sc} and FF in the IDTTIC based devices.

2.3. Transistors performance of NFAs

Following the highly-order GIWAXS patterns of IDTIC and IDTTIC (strong crystallinity), we further investigated a broader application of these two materials in field-effect transistor devices. Top-gate, bottom-contact OFET devices were fabricated to investigate the semiconducting properties of IDTTIC and IDTIC. Experimental details are shown in Supporting Information. IDTIC and IDTTIC thin films were annealed at either 80, 100, 130 and 150 °C. Significantly, all devices exhibited n-channel characteristics, with well-defined saturation regimes (Figure 5 and Figure S16). The optimized performance of IDTIC was obtained at 100 °C, showing a high threshold voltage of 45.3 V with a linear and saturation mobility of 0.12 and 0.15 $\text{cm}^2\text{V}^{-1}\text{s}^{-1}$, respectively (Figure 5 a,c). In contrast, IDTTIC based devices delivered an improved mobility (linear mobility: 0.45 $\text{cm}^2\text{V}^{-1}\text{s}^{-1}$ and saturation mobility: 0.5 $\text{cm}^2\text{V}^{-1}\text{s}^{-1}$) and lower threshold voltage of 21 V in the optimized conditions (130 °C annealing for 5 min), as depicted in Figure 5 b,d. These results indicate that the conjugated core unit has a crucial influence on the carrier transport property of FREA-type semiconductors.

3. Conclusion

This article is protected by copyright. All rights reserved.

In conclusion, we have successfully synthesized a new n-type small molecule semiconductor IDTTIC and incorporated it as an electron acceptor in OSCs and n-type top gate bottom contact OFETs. When blended with PBDB-T to form the photoactive layer, IDTTIC-based solar cells delivered a power conversion efficiency of 11.2% without any post-annealing treatment; in contrast to 5.67% PBDB-T:IDTIC devices. The low performance obtained in IDTIC solar cells was attributed to reduced charge generation and transport properties due to trap-assisted recombination that limits both FF and J_{sc} values. Morphological characterizations revealed that both of these FREA materials present high order of crystallinity. However, extending the small molecule core in the SM lead to an increase in both the coherence length and the domain purity in PBDB-T: IDTTIC blends, which was beneficial for the improved carrier generation and transport. In comparison with IDTIC, the extended core of IDTTIC resulted in a higher electron mobility ($0.50 \text{ cm}^2\text{V}^{-1}\text{s}^{-1}$) compared to IDTIC ($0.15 \text{ cm}^2\text{V}^{-1}\text{s}^{-1}$) in OFET devices. Our results demonstrate that the extended π -conjugation of backbone with more thiophene rings can be a beneficial strategy to improve the power conversion efficiency of OSC and the charge mobility of OFET devices.

Supporting Information ((delete if not applicable))

Supporting Information is available from the Wiley Online Library or from the author.

4. Acknowledgments

This article is protected by copyright. All rights reserved.

D. Baran acknowledges KAUST Solar Center Competitive Fund (CCF) for financial support.

GIWAXS/R-SoXS measurements and analysis by M. M. Nahid and H. Ade are supported by ONR grant N00141512322 and KAUST's Center Partnership Fund (No. 3321). X-ray data were acquired at beamlines 7.3.3 and 11.0.1.2 at the Advanced Light Source (ALS) in Berkeley National Lab, which is supported by the U.S. Department of Energy (DE-AC02-05CH11231). Z. Peng, S. Stuard, and I. Angunawela assisted with part of the R-SoXS data acquisition. C. Wang, C. Zhu, A.L.D. Kilcoyne, and E. Schaible are acknowledged for the beamline support.

Received: ((will be filled in by the editorial staff))

Revised: ((will be filled in by the editorial staff))

Published online: ((will be filled in by the editorial staff))

References

- [1] X. Guo, A. Facchetti, T. J. Marks, *Chem. Rev.* **2014**, *114*, 8943.
- [2] Y. Wang, Z. Yan, H. Guo, M. A. Uddin, S. Ling, X. Zhou, H. Su, J. Dai, H. Y. Woo, X. Guo, *Angew. Chemie Int. Ed.* **2017**, *56*, 15304.
- [3] C. Zhang, Y. Zang, E. Gann, C. R. McNeill, X. Zhu, C. A. Di, D. Zhu, *J. Am. Chem. Soc.* **2014**, *136*, 16176.
- [4] H. Yan, Z. Chen, Y. Zheng, C. Newman, J. R. Quinn, F. Dötz, M. Kastler, A. Facchetti, *Nature* **2009**, *457*, 679.

This article is protected by copyright. All rights reserved.

- [5] L. E. Polander, S. P. Tiwari, L. Pandey, B. M. Seifried, Q. Zhang, S. Barlow, C. Risko, J. L. Brédas, B. Kippelen, S. R. Marder, *Chem. Mater.* **2011**, *23*, 3408.
- [6] Y. Lin, Q. He, F. Zhao, L. Huo, J. Mai, X. Lu, C. J. Su, T. Li, J. Wang, J. Zhu, Y. Sun, C. Wang, X. Zhan, *J. Am. Chem. Soc.* **2016**, *138*, 2973.
- [7] H. Bin, L. Gao, Z. G. Zhang, Y. Yang, Y. Zhang, C. Zhang, S. Chen, L. Xue, C. Yang, M. Xiao, Y. Li, *Nat. Commun.* **2016**, *7*, 13651.
- [8] B. Kan, H. Feng, X. Wan, F. Liu, X. Ke, Y. Wang, Y. Wang, H. Zhang, C. Li, J. Hou, Y. Chen, *J. Am. Chem. Soc.* **2017**, *139*, 4929.
- [9] N. Gasparini, A. Wadsworth, M. Moser, D. Baran, I. McCulloch, C. J. Brabec, *Adv. Energy Mater.* **2018**, *11*, 1703298.
- [10] H. Cha, J. Wu, A. Wadsworth, J. Nagitta, S. Limbu, S. Pont, Z. Li, J. Searle, M. F. Wyatt, D. Baran, J. S. Kim, I. McCulloch, J. R. Durrant, *Adv. Mater.* **2017**, *29*, 1701159.
- [11] J. Zhao, Y. Li, G. Yang, K. Jiang, H. Lin, H. Ade, W. Ma, H. Yan, *Nat. Energy* **2016**, *1*, 15027.
- [12] N. Gasparini, L. Lucera, M. Salvador, M. Prosa, G. D. Spyropoulos, P. Kubis, H.-J. Egelhaaf, C. J. Brabec, T. Ameri, *Energy Environ. Sci.* **2017**, *10*, 885.
- [13] C. B. Nielsen, S. Holliday, H.-Y. Chen, S. J. Cryer, I. McCulloch, *Acc. Chem. Res.* **2015**, *48*, 2803.
- [14] Y. J. Hwang, H. Li, B. A. E. Courtright, S. Subramaniyan, S. A. Jenekhe, *Adv. Mater.* **2016**, *28*, 124.
- [15] G. E. Park, H. J. Kim, S. Choi, D. H. Lee, M. A. Uddin, H. Y. Woo, M. J. Cho, D. H. Choi, *Chem.*

This article is protected by copyright. All rights reserved.

Commun. **2016**, *52*, 8873.

- [16] Q. Wu, D. Zhao, A. M. Schneider, W. Chen, L. Yu, *J. Am. Chem. Soc.* **2016**, *138*, 7248.
- [17] A. Tang, C. Zhan, J. Yao, E. Zhou, *Adv. Mater.* **2017**, *29*, 1600013.
- [18] D. Baran, T. Kirchartz, S. Wheeler, S. Dimitrov, M. Abdelsamie, J. Gorman, R. S. Ashraf, S. Holliday, A. Wadsworth, N. Gasparini, P. Kaienburg, H. Yan, A. Amassian, C. J. Brabec, J. R. Durrant, I. McCulloch, *Energy Environ. Sci.* **2016**, *9*, 3783.
- [19] N. Gasparini, M. Salvador, S. Strohm, T. Heumueller, I. Levchuk, A. Wadsworth, J. H. Bannock, J. C. de Mello, H.-J. Egelhaaf, D. Baran, I. McCulloch, C. J. Brabec, *Adv. Energy Mater.* **2017**, *7*, 1700770.
- [20] D. Baran, R. S. Ashraf, D. A. Hanifi, M. Abdelsamie, N. Gasparini, J. A. Röhr, S. Holliday, A. Wadsworth, S. Lockett, M. Neophytou, C. J. M. Emmott, J. Nelson, C. J. Brabec, A. Amassian, A. Salleo, T. Kirchartz, J. R. Durrant, I. McCulloch, *Nat. Mater.* **2017**, *16*, 363.
- [21] W. Zhao, S. Li, H. Yao, S. Zhang, Y. Zhang, B. Yang, J. Hou, *J. Am. Chem. Soc.* **2017**, *139*, 7148.
- [22] Y. Cui, H. Yao, B. Gao, Y. Qin, S. Zhang, B. Yang, C. He, B. Xu, J. Hou, *J. Am. Chem. Soc.* **2017**, *139*, 7302.
- [23] S. Zhang, Y. Qin, J. Zhu, J. Hou, *Adv. Mater.* **2018**, *30*, 1800868.
- [24] W. Zhao, D. Qian, S. Zhang, S. Li, O. Inganäs, F. Gao, J. Hou, *Adv. Mater.* **2016**, *28*, 4734.
- [25] Y. Lin, F. Zhao, Q. He, L. Huo, Y. Wu, T. C. Parker, W. Ma, Y. Sun, C. Wang, D. Zhu, A. J. Heeger, S. R. Marder, X. Zhan, *J. Am. Chem. Soc.* **2016**, *138*, 4955.

This article is protected by copyright. All rights reserved.

- [26] S. Dai, F. Zhao, Q. Zhang, T.-K. Lau, T. Li, K. Liu, Q. Ling, C. Wang, X. Lu, W. You, X. Zhan, *J. Am. Chem. Soc.* **2017**, *139*, 1336.

- [27] X. Shi, L. Zuo, S. B. Jo, K. Gao, F. Lin, F. Liu, A. K.-Y. Jen, *Chem. Mater.* **2017**, *29*, 8369.
- [28] S. Holliday, R. S. Ashraf, A. Wadsworth, D. Baran, S. A. Yousaf, C. B. Nielsen, C.-H. Tan, S. D. Dimitrov, Z. Shang, N. Gasparini, M. Alamoudi, F. Laquai, C. J. Brabec, A. Salleo, J. R. Durrant, I. McCulloch, *Nat. Commun.* **2016**, *7*, 11585.

- [29] F. Yang, C. Li, W. Lai, A. Zhang, H. Huang, W. Li, *Mater. Chem. Frontiers.* **2017**, *1*, 1389.

- [30] W. Zhang, J. Smith, S. Watkins, R. Gysel, M. Mcgehee, A. Salleo, J.Kirkpatrick, S. Ashraf, T. Anthopoulos, M. Heeney, I. McCulloch *J. Am. Chem. Soc.* **2010**, *132*, 11437.

- [31] W. Zhang, Y. Han, X. Zhu, Z. Fei, Y. Feng, N. D. Treat, H. Faber, N. Stingelin, I. McCulloch, T. D. Anthopoulos, M. Heeney, *Adv. Mater.* **2016**, *28*, 3922.

- [32] J. Wang, W. Wang, X. Wang, Y. Wu, Q. Zhang, C. Yan, W. Ma, W. You, X. Zhan, *Adv. Mater.* **2017**, *29*, 1702125.

- [33] B. Jia, S. Dai, Z. Ke, C. Yan, W. Ma, X. Zhan, *Chem. Mater.* **2017**, *30*, 239.

- [34] Z.-G. Zhang, Y. Yang, J. Yao, L. Xue, S. Chen, X. Li, W. Morrison, C. Yang, Y. Li, *Angew. Chemie Int. Ed.* **2017**, *56*, 13503.

- [35] J. L. Wang, Q. R. Yin, J. S. Miao, Z. Wu, Z. F. Chang, Y. Cao, R. B. Zhang, J. Y. Wang, H. Bin Wu, Y. Cao, *Adv. Funct. Mater.* **2015**, *25*, 3514.

- [36] J. L. Brédas, *Chem. Mater.* **2017**, *29*, 477.

This article is protected by copyright. All rights reserved.

[37] X. Xu, Z. Bi, W. Ma, Z. Wang, W. C. H. Choy, W. Wu, G. Zhang, Y. Li, Q. Peng, *Adv. Mater.* **2018**,

30, 1703973.

[38] M. M. Mandoc, F. B. Kooistra, J. C. Hummelen, B. de Boer, P. W. M. Blom, *Appl. Phys. Lett.* **2007**, 91, 263505.

[39] W. L. Leong, S. R. Cowan, A. J. Heeger, *Adv. Energy Mater.* **2011**, 1, 517.

[40] N. A. Ran, J. A. Love, M. C. Heiber, X. Jiao, M. P. Hughes, A. Karki, M. Wang, V. V. Brus, H. Wang, D. Neher, H. Ade, G. C. Bazan, T.-Q. Nguyen, *Adv. Energy Mater.* **2017**, 7, 1701073.

[41] Y. Ma, M. Zhang, Y. Yan, J. Xin, T. Wang, W. Ma, C. Tang, Q. Zheng, *Chem. Mater.* **2017**, 29, 7942.

[42] X. Song, N. Gasparini, D. Baran, *Adv. Electron. Mater.* **2017**, 3, 1700358.

[43] N. Gasparini, X. Jiao, T. Heumueller, D. Baran, G. J. Matt, S. Fladischer, E. Spiecker, H. Ade, C. J. Brabec, T. Ameri, *Nat. Energy* **2016**, 1, 16118.

[44] C. G. Shuttle, B. O'Regan, A. M. Ballantyne, J. Nelson, D. D. C. Bradley, J. de Mello, J. R. Durrant, *Appl. Phys. Lett.* **2008**, 92, 93311.

[45] S. Sandén, N. M. Wilson, O. J. Sandberg, R. Österbacka, *Appl. Phys. Lett.* **2016**, 108, 193301.

[46] H. Hu, K. Jiang, P. C. Y. Chow, L. Ye, G. Zhang, Z. Li, J. H. Carpenter, H. Ade, H. Yan, *Adv. Energy Mater.* **2017**, 7, 1701674.

[47] S. Mukherjee, A. A. Herzing, D. Zhao, Q. Wu, L. Yu, H. Ade, D. M. DeLongchamp, L. J. Richter, *J. Mater. Res.* **2017**, 32, 1921.

This article is protected by copyright. All rights reserved.

- [48] X. Jiao, L. Ye, H. Ade, *Adv. Energy Mater.* **2017**, *7*, 1700084.
- [49] E. Gann, A. T. Young, B. A. Collins, H. Yan, J. Nasiatka, H. A. Padmore, H. Ade, A. Hexemer, C. Wang, *Rev. Sci. Instrum.* **2012**, *83*, 45110.
- [50] M. M. Nahid, R. Matsidik, A. Welford, E. Gann, L. Thomsen, M. Sommer, C. R. McNeill, *Adv. Funct. Mater.* **2017**, *27*, 1604744.
- [51] S. Li, L. Ye, W. Zhao, S. Zhang, S. Mukherjee, H. Ade, J. Hou, *Adv. Mater.* **2016**, *28*, 9423.
- [52] E. Gann, B. A. Collins, M. Tang, J. R. Tumbleston, S. Mukherjee, H. Ade, *J. Synchrotron Radiat.* **2016**, *23*, 219.
- [53] L. Ye, H. Hu, M. Ghasemi, T. Wang, B. A. Collins, J.-H. Kim, K. Jiang, J. H. Carpenter, H. Li, Z. Li, T. McAfee, J. Zhao, X. Chen, J. L. Y. Lai, T. Ma, J.-L. Bredas, H. Yan, H. Ade, *Nat. Mater.* **2018**, *17*, 253.
- [54] L. Ye, X. Jiao, S. Zhang, H. Yao, Y. Qin, H. Ade, J. Hou, *Adv. Energy Mater.* **2017**, *7*, 1601138.

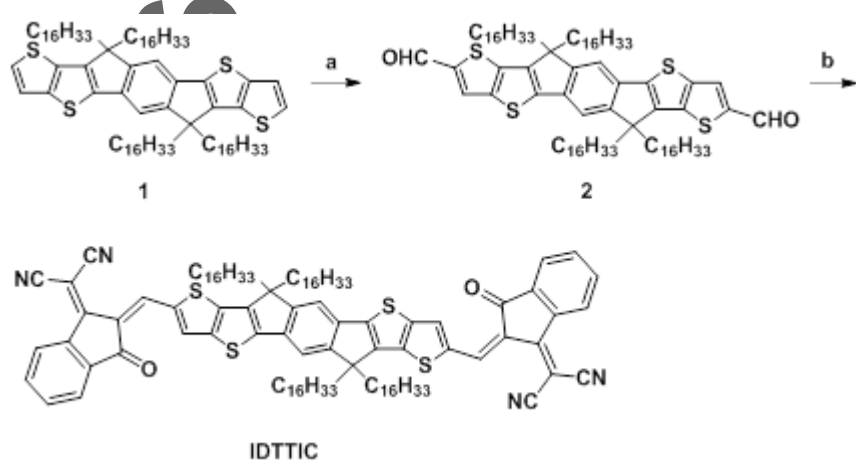
Author Manuscript

This article is protected by copyright. All rights reserved.

Figures:

Author manuscript

iScript



Scheme 1 Synthesis of C₁₆-IDTTIC. a. POCl₃, DMF, CHCl₃, 81%; b. (3-dihydro-1H-inden-1-ylidene)malononitrile, pyridine, CHCl₃, 23%.

This article is protected by copyright. All rights reserved.

ipt
Author

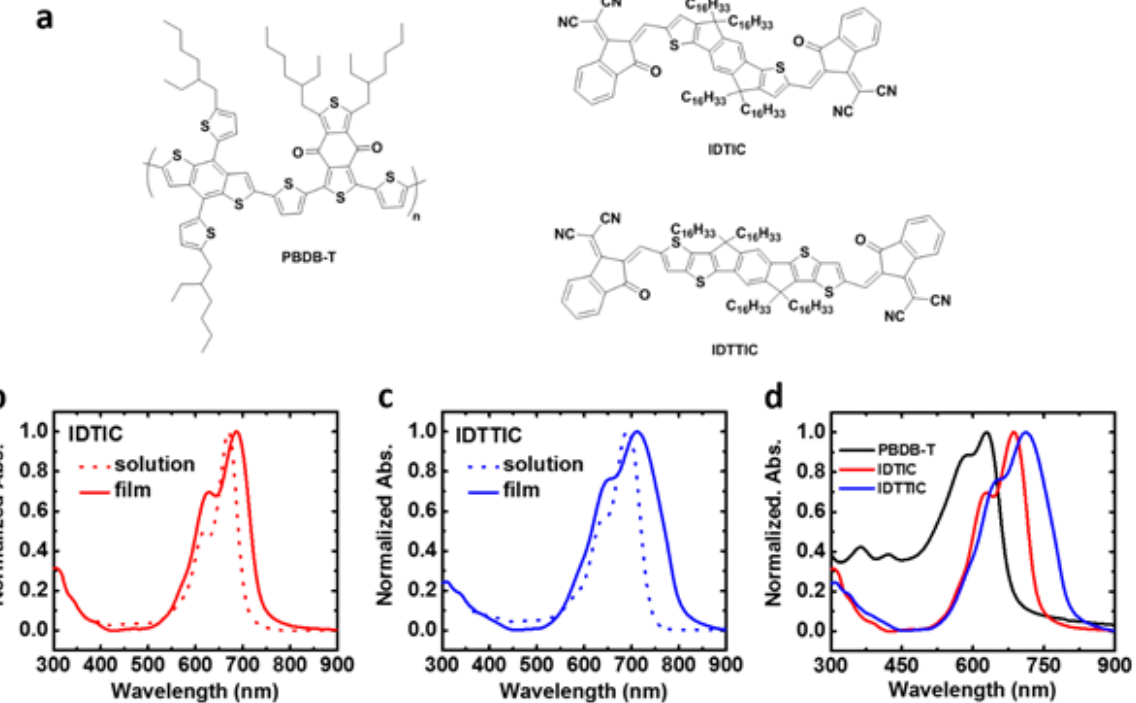


Figure 1. a) Chemical structures of PBDB-T, IDTIC and IDTTIC. b) and c) Normalized UV-Vis-NIR absorption spectra of IDTIC and IDTTIC in chloroform and of thin film. d) Normalized thin-film absorption curves of PBDB-T, IDTIC and IDTTIC.

This article is protected by copyright. All rights reserved.

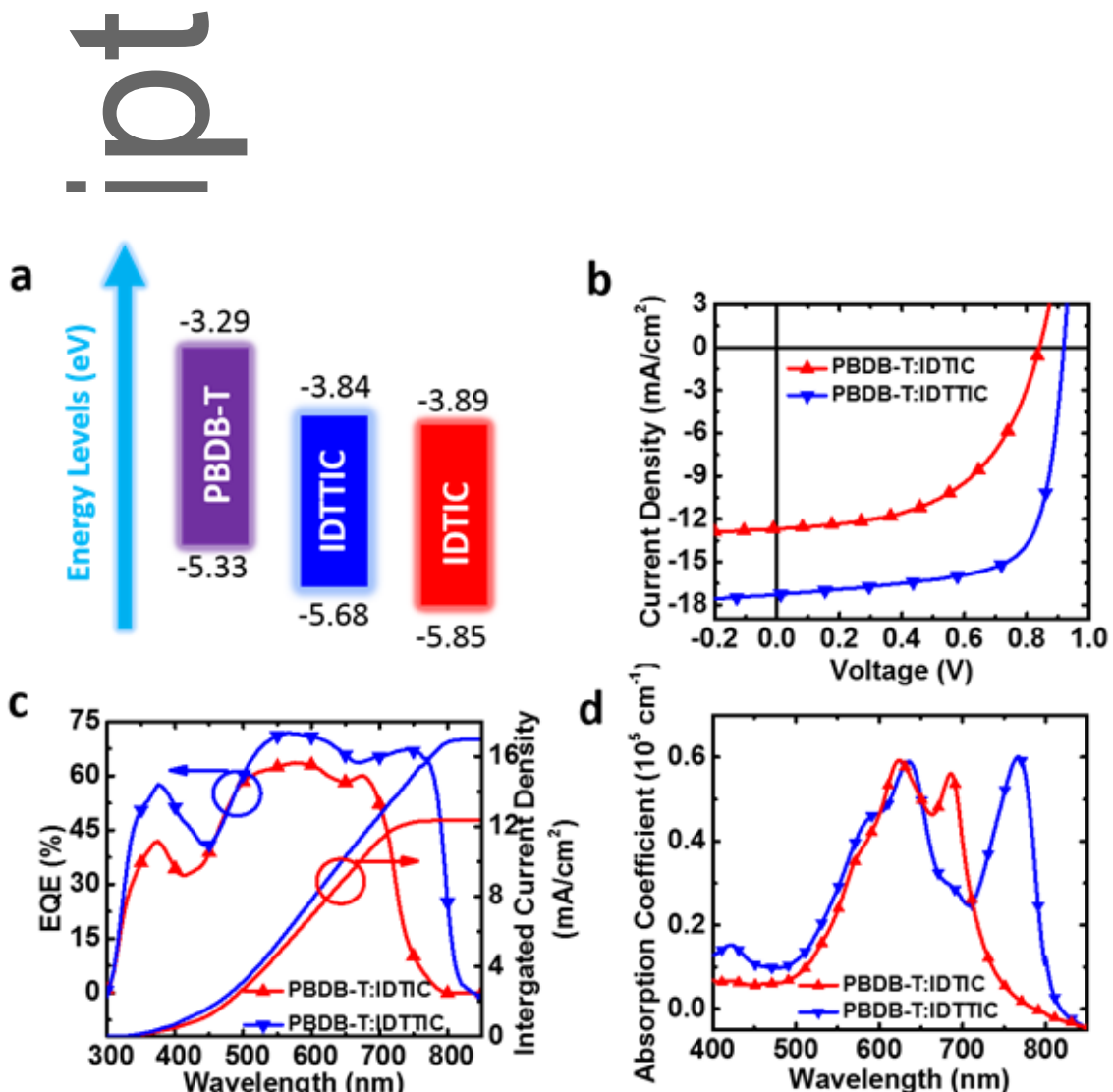


Figure 2. a) Energy levels of PBDB-T, IDTTIC and IDTIC. b) J-V curves of the best performing devices. c) EQE curves of the corresponding devices (left side) and integrated current densities (right side). d) Absorption coefficients of blend film (PBDB-T:IDTTIC, PBDB-T:IDTIC).

This article is protected by copyright. All rights reserved.

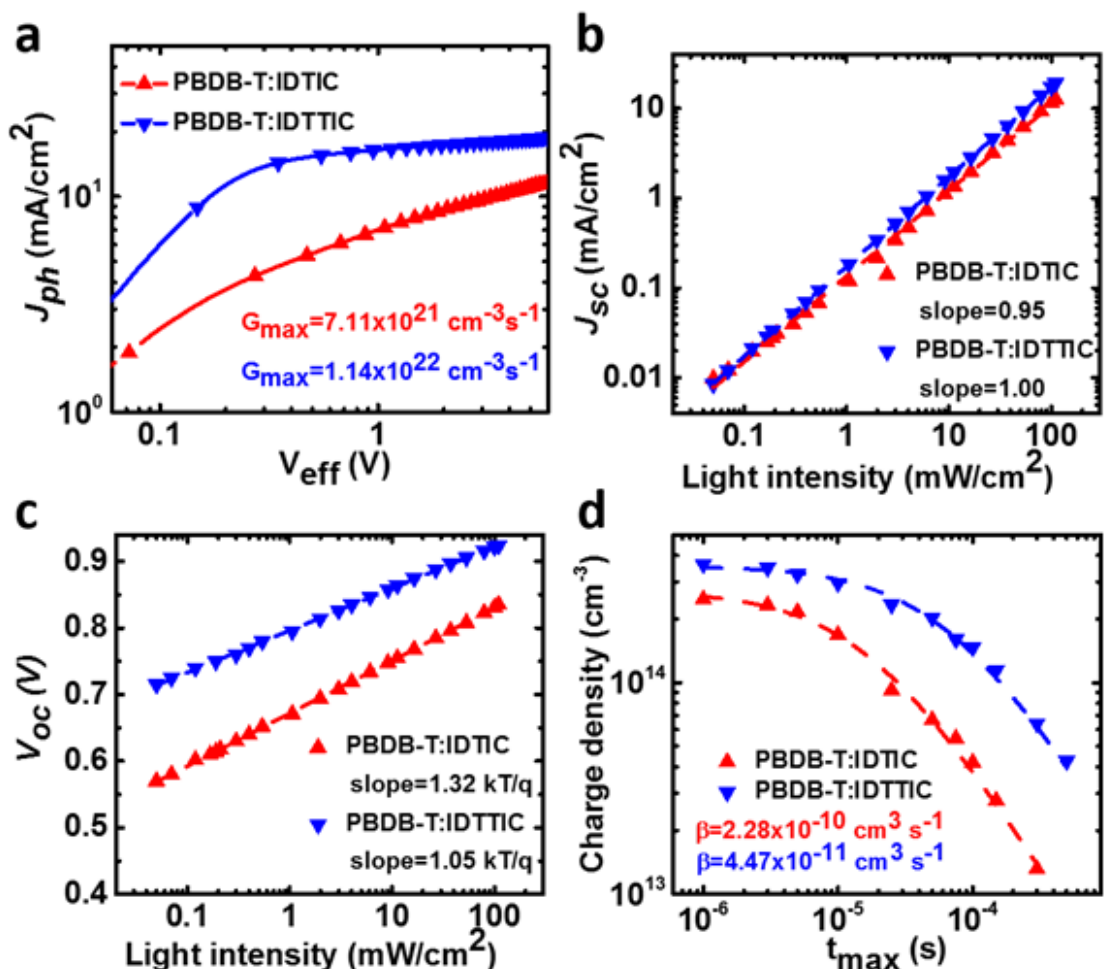
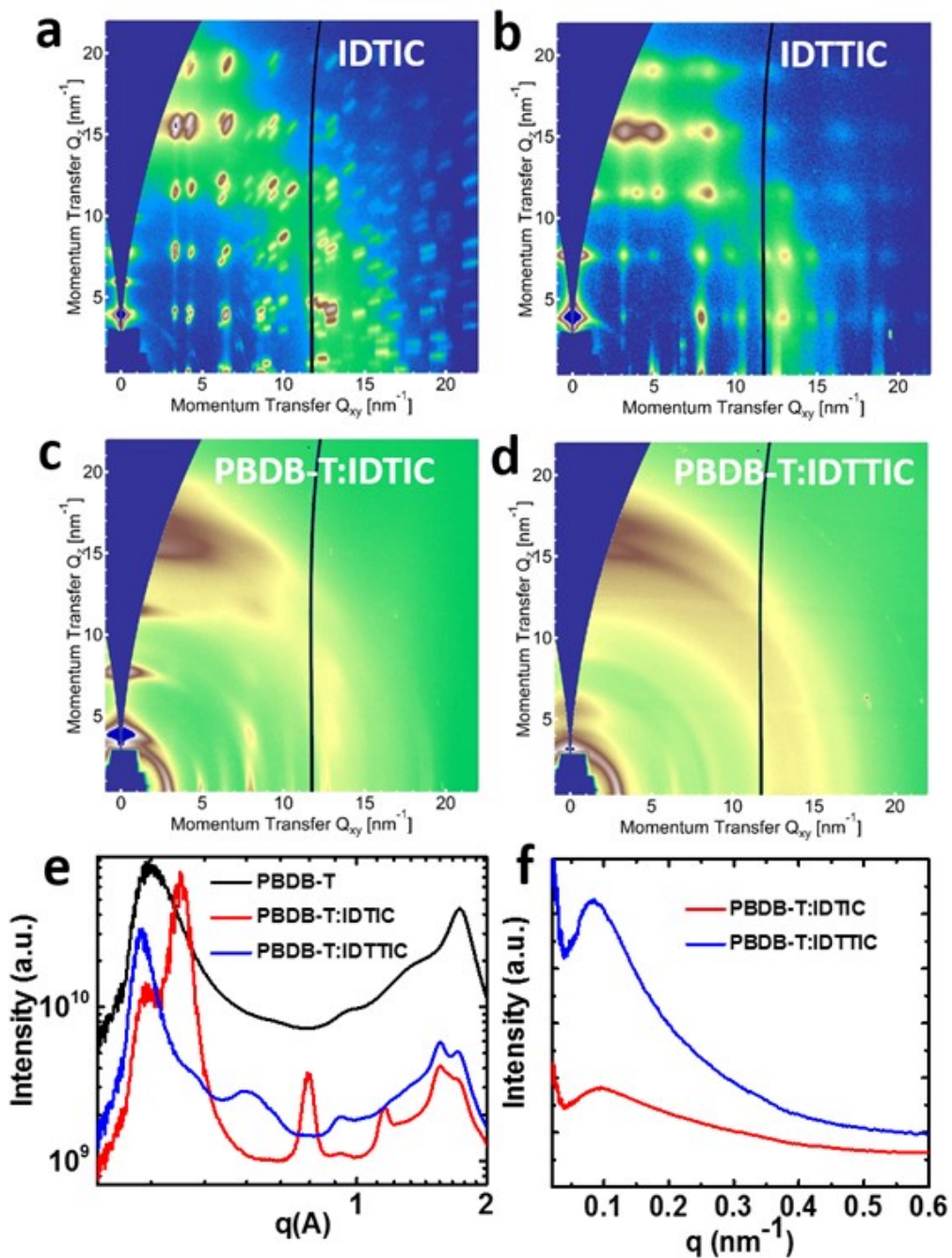


Figure 3. a): Photocurrent density as a function of the effective voltage at 100 mW/cm² illumination. Short-circuit current density (b) and open-circuit voltage (c) under different light intensity of PBDB-T:IDTTIC and PBDB-T:IDTIC devices. d) Charge carrier density as a function of delay time (t_d) extracted from photo-CELIV measurements. The fitting curves are according to equation 1.

Author

This article is protected by copyright. All rights reserved.



Aut

This article is protected by copyright. All rights reserved.

Figure 4. GIWAXS patterns of (a) neat IDTIC and (b) IDTTIC, and blend (c) PBDB-T:IDTIC and (d) PBDB-T:IDTTIC films. (e) GIWAXS 1D out of plane (OOP) profiles and (f) contrast and thickness normalized Lorentz corrected R-SoXS profiles of the blend films based on PBDB-T:IDTIC and PBDB-T:IDTTIC.

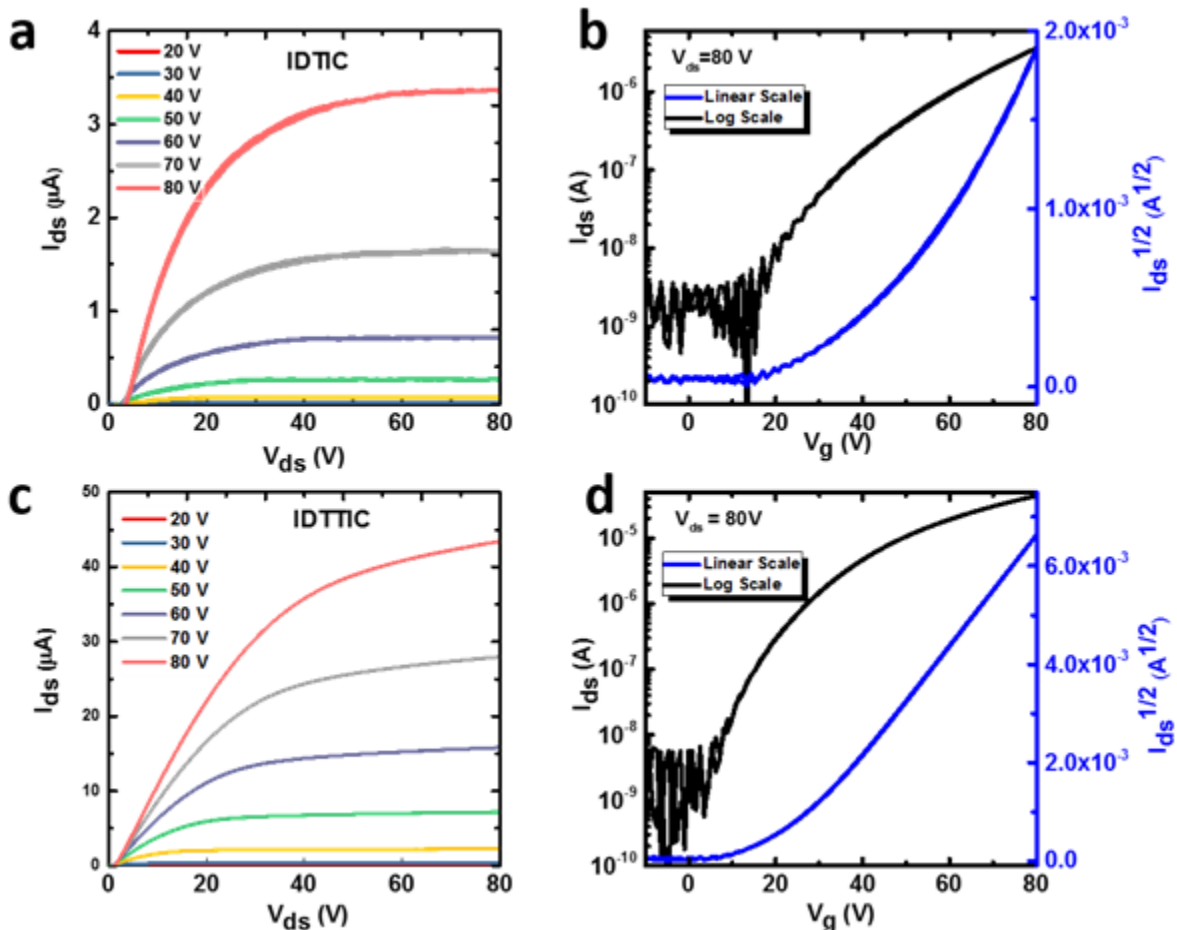


Figure 5. Output (a) and transfer (b) characteristics of IDTIC top-gate, bottom-contact transistor device annealed at 100 °C for 5 minutes, yield $\mu_{\text{sat}} = 0.15 \text{ cm}^2/\text{Vs}$ and $V_{\text{th}} = 45.3 \text{ V}$. Output (c) and transfer (d) characteristics of IDTTIC top-gate, bottom-contact transistor device annealed at 130 °C

for 5 minutes, yields, $\mu_{\text{sat}} = 0.50 \text{ cm}^2/\text{Vs}$ and $V_{\text{th}} = 21.0 \text{ V}$. Note. All devices used a channel L = 50 μm and a W = 1000 μm .

Author
Manuscript

Table 1. Photovoltaic parameter of OSCs based on PBDB-T:IDTTIC and PBDB-T:IDTIC

Blend Film	J_{sc} (mA/cm ²)	Integrated J_{sc} (mA/cm ²)	V_{oc} (mV)	FF (%)	PCE (%)	Ave PCE (%) ^a	$\mu_{\text{h}}^{\text{b}}$ (cm ² V ⁻¹ s ⁻¹)	$\mu_{\text{e}}^{\text{b}}$ (cm ² V ⁻¹ s ⁻¹)	$\mu_{\text{e}}/\mu_{\text{h}}$
PBDB-T:IDTIC	12.7	12.4	840	56.3	5.67	5.34	2.56×10^{-4}	5.51×10^{-5}	0.21
PBDB-T:IDTTIC	17.3	16.9	919	70.4	11.2	10.7	3.38×10^{-4}	1.15×10^{-4}	0.34

^a Average PCE values obtained from 10 devices. ^b Carrier mobility values measured from SCLC method.

Author
Manuscript

This article is protected by copyright. All rights reserved.

Table 2. GIWAXS and R-SoXS parameters of PBDB-T:IDTIC and PBDB-T:IDTTIC blend films.

Sample	GIWAXS		R-SoXS	
	NFAs OOP π - π stacking d-spacing (nm)	NFAs OOP π - π stacking coherence Length (nm)	Center-to-Center Spacing (nm) [@284.2 eV]	Relative mean square composition variations [@284.2 eV]
PBDB-T: IDTIC	0.392	1.35 (± 0.02)	80.60	0.42
PBDB-T: IDTTIC	0.389	4.60 (± 0.11)	84.88	1.00

The table of contents :

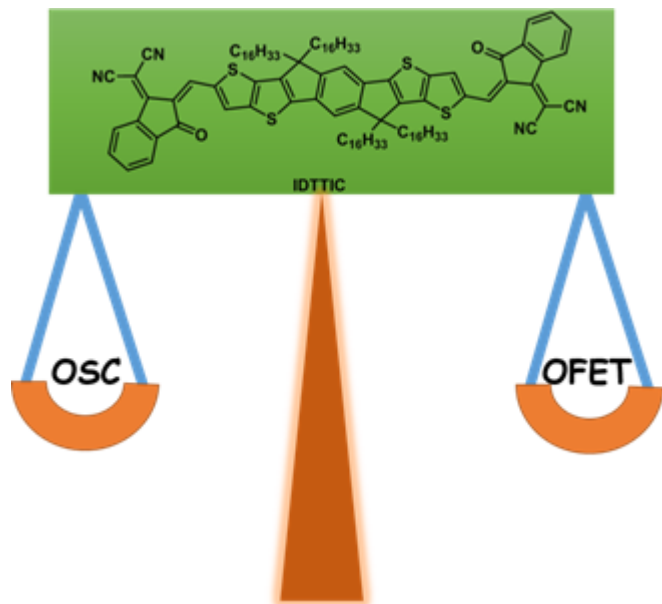
Indacenodithieno[3,2-b]thiophene (IDTT) core unit with linear alkylated sidechain (C_{16}) based n-type small-molecule semiconductor, IDTTIC, was synthesized and characterized for OSCs and OFETs applications. Compared to IDTIC, IDTTIC with the extended backbone featured a higher mobility ($0.50\text{ cm}^2\text{ V}^{-1}\text{ s}^{-1}$) and photo-to-current efficiency with commonly used donor PBDB-T (11.2%), which is due to the high ordered packing, enhanced absorption coefficient and decreased recombination loss.

This article is protected by copyright. All rights reserved.

Keywords: Fused-ring small molecule, Organic Solar Cells, Organic field-effect transistors, Non-fullerene acceptor, high efficiency

Xin Song,¹ Nicola Gasparini,^{*1} Masrur Morshed Nahid,² Hu Chen,¹ Sky Marie Macphee,¹ Weimin Zhang,¹ Victoria Norman,³ Chenhui Zhu,³ Daniel Bryant,¹ Harald Ade,² Iain McCulloch,^{,4} Derya Baran^{*1}

Highly Crystalline Fused-Ring n-Type Small Molecule for Non-Fullerene Acceptor Based Organic Solar Cells and Field-Effect Transistors



This article is protected by copyright. All rights reserved.